NJC

PAPER

View Article Online
View Journal | View Issue

Cite this: *New J. Chem.*, 2017, **41**, 11016

Substituent effects on the basicity (pK_a) of aryl guanidines and 2-(arylimino)imidazolidines: correlations of pH-metric and UV-metric values with predictions from gas-phase *ab initio* bond lengths†

Christophe Dardonville,*[a] Beth A. Caine,[bc] Marta Navarro de la Fuente,[a] Guillermo Martín Herranz,[a] Beatriz Corrales Mariblanca[a] and Paul L. A. Popelier[bc]

Received 10th July 2017,
Accepted 28th July 2017

DOI: 10.1039/c7nj02497e

rsc.li/njc

The dissociation constants of two related series of 2-(arylimino)imidazolidine and aryl guanidine α_2-adrenoceptor antagonists (35 compounds in total) were measured by potentiometric titrations and by UV-spectrophotometry using the 96-well microtitre plate method. The experimental values obtained using both methods were quite consistent and showed a very good agreement with the pK_a values calculated using the AIBLHiCoS methodology, which uses only a single bond length obtained using *ab initio* calculations at a low level of theory. The prediction power of the imidazolidine and guanidine set of compounds was very good with deviations typically <0.30 and <0.24 pK_a units, and a mean absolute error (MAE) of 0.23 and 0.29, respectively. The study of the quantitative effect of diverse substituents on the basicity of aryl guanidine and 2-(arylimino)imidazolidine derivatives is useful for medicinal chemists working with biologically relevant guanidine-containing molecules.

1. Introduction

The guanidine group of the amino acid arginine is ubiquitous in Nature. In its protonated state, several resonance forms that delocalize the cationic charge of the guanidinium cation over the entire functional group contribute to the high basicity of guanidine (pK_{aH} = 13.6 in water).[1] The H-bonding ability of guanidine makes this group a valuable tool for the design of compounds for different pharmacological applications such as DNA binding drugs (*e.g.* anticancer and antiprotozoal agents),[2–11] analgesic compounds,[12–14] α_1-noradrenaline receptors (*e.g.* α_1-AR antagonists for the treatment of benign prostate hyperplasia),[15] or α_2-AR modulators for neuropsychiatric therapies.[16–19]

Centrally acting α_2-adrenoceptor antagonists are potentially useful pharmacological tools for the treatment of depression and schizophrenia.[16] Among these, arylguanidines and 2-(arylimino)-imidazolidines represent an important family of α-adrenoceptor modulators.[16–20] The prototypical example of a (phenylimino)-imidazolidine drug is α_2-AR and imidazoline receptor agonist clonidine (*i.e.* *N*-(2,6-dichlorophenyl)-4,5-dihydro-1*H*-imidazol-2-amine) used, among other applications, as an antihypertensive drug and for controlling neuropathic pain (Fig. 1).[21] As both the guanidine and 2-aminoimidazoline groups are strong bases, they are protonated at physiological pH. Thus, this physicochemical property may impair the absorption and/or limit the uptake of guanidine-containing molecules through biological membranes, including the blood–brain barrier,[22,23] a drawback that is highly relevant for centrally acting drugs.

The protonation state of a drug molecule determines its lipophilicity, solubility in biological fluids, ability to cross biological membranes, degree of protein binding, and its capacity to bind to biological targets. Hence, knowing the dissociation constants (pK_a) of drugs is crucial because this parameter affects the key pharmacokinetic properties such as administration, distribution, metabolism and excretion (ADME).[24]

One of the objectives of this work is to understand the quantitative effect of diverse substituents on the aqueous basicity of pharmacologically important families of compounds: aryl guanidines and 2-(arylimino)imidazolidines. This knowledge is useful to assist in the design of new biologically relevant guanidine-containing molecules with improved pharmacokinetic properties.[22] Another objective is to compare the experimental pK_a values of these series with those obtained by *ab initio* calculations using the AIBLHiCoS method.[25,26] The Ab Initio Bond Lengths High Correlation Subsets protocol works on the basis that, for a series of electronically congeneric compounds, chemical space

[a] *Instituto de Química Médica, IQM-CSIC, Juan de la Cierva 3, E-28006 Madrid, Spain. E-mail: dardonville@iqm.csic.es; Fax: +34 915644853; Tel: +34 912587490*
[b] *Manchester Institute of Biotechnology (MIB), 131 Princess Street, Manchester, M1 7DN, UK*
[c] *School of Chemistry, Univ. of Manchester, Oxford Road, Manchester M13 9PL, UK*

† Electronic supplementary information (ESI) available: Excel sheet template for the data analysis of UV-metric pK_a determination. Tables S1–S6 and Fig. S1–S4. ^{1}H and ^{13}C NMR spectra of compounds **1a** and **11a–15a**. See DOI: 10.1039/c7nj02497e

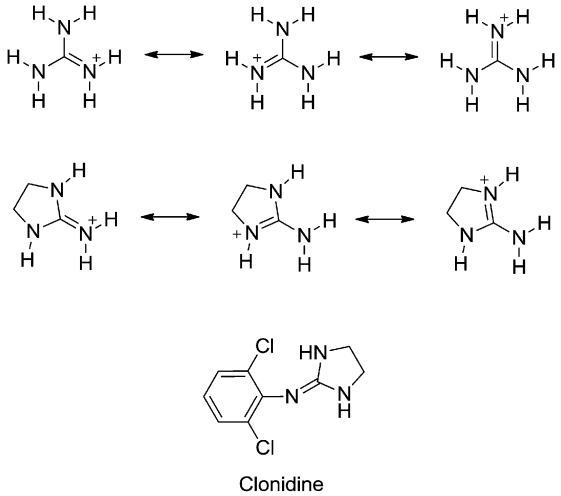

Fig. 1 Resonance forms of the guanidinium and 2-iminoimidazolidinium cations responsible for the high basicity of these functional groups. Structure of the archetypal 2-(arylimino)imidazolidine drug clonidine.

may be partitioned according to a linear free energy relationship (LFER) between the calculated gas-phase equilibrium bond lengths and aqueous pK_a values. The equations resulting from highly correlated, local linear relationships for structurally similar molecules are then used as predictive models for calculating the pK_a values of other compounds belonging to the appropriate High Correlation Subset (HiCoS). In this work, using a specific bond length and tautomeric form in the neutral state, we have constructed one predictive model with a training set of 13 guanidines and a second model with a training set of 23 2-(phenylimino)imidazolidines. This method is a valuable tool that has already proven its power for the accurate determination of pK_as of other guanidine-containing drugs in addition to a number of other functional groups.[25,27–29] However, this method has not been tested, until now, with the medically relevant 2-(phenylimino)imidazolidine scaffold. The predictive models built with these series show that the AIBLHiCoS method is an accurate pK_a prediction tool with this pharmacologically important family of compounds.

2. Results and discussion

2.1. Synthesis

Trifluoroacetate salts of phenylguanidines (**1b**, **2b**, **3b**, **6b**, **7b**, and **24–27b**) and 2-(phenylimino)imidazolidines (**2a–10a**, and **23a**) were synthesized from their Boc-protected precursors using CF_3CO_2H/CH_2Cl_2 as reported (Scheme 1).[7] These Boc-protected precursors were obtained by a reaction of the corresponding anilines with *N*,*N*′-bis-(*tert*-butoxycarbonyl)imidazolidin-2-thione or *N*,*N*′-bis(*tert*-butoxycarbonyl)thiourea and $HgCl_2/Et_3N/DMF$.[7] The pyridino derivatives **17–22** were synthesized as hydrochloride

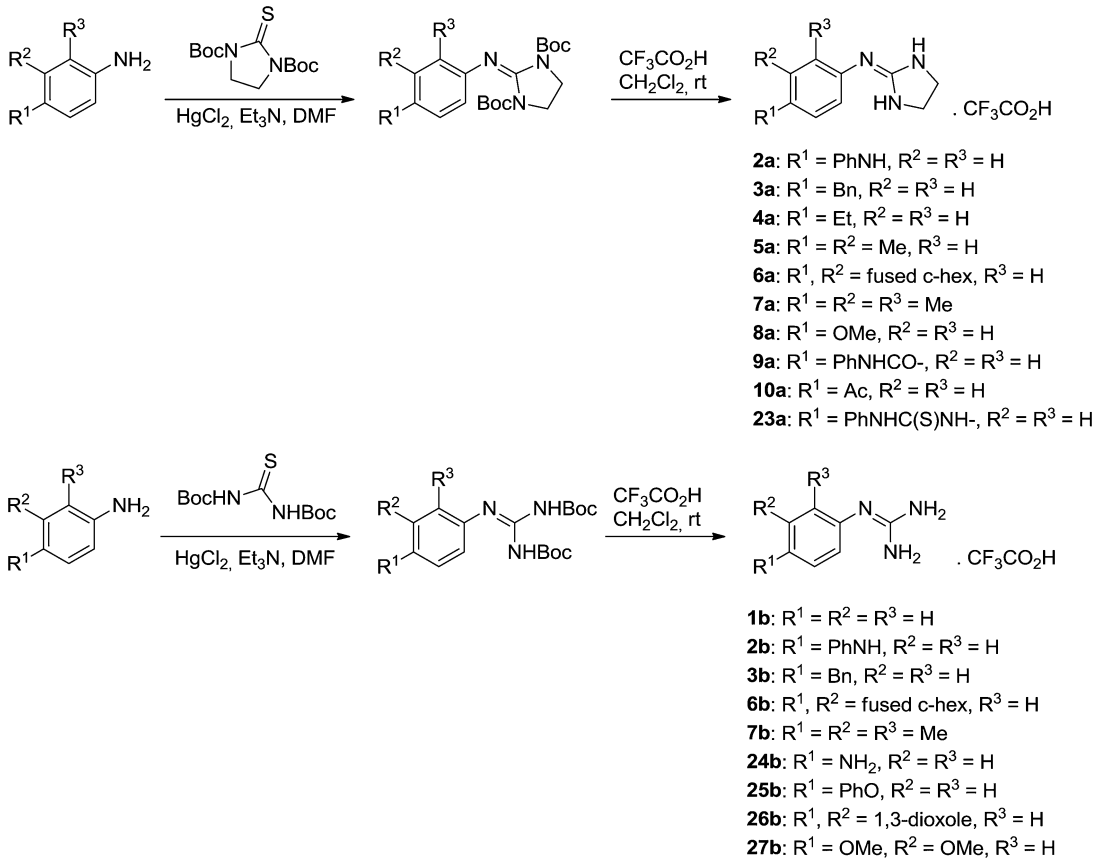

Scheme 1 Synthesis of **2a–10a**, **23a**, **1b–3b**, **6b**, **7b**, and **24b–27b**.

salts by Rozas and co-workers following a procedure similar to that shown in Scheme 1.[30]

Compounds **1a** and **11a–15a** were synthesized as shown in Scheme 2 following the procedure of Mundla *et al.*[31]

2.2. Correlation between experimental pH-metric, UV-metric, and calculated pK_a

The pK_a values of two sets of 23 2-(arylimino)imidazolidines (**1a–23a**) and 12 arylguanidines (**1b**, **2b**, **3b**, **6b**, **7b**, **17b**, **18b**, **22b–27b**), most of them developed by Rozas and co-workers as α_2-adrenoceptor ligands,[16–20] were measured by potentiometric titration (*i.e.* pH-metric) at 25 °C using the Sirius T3 apparatus, and by spectrophotometry (*i.e.* UV-metric) using the 96-well microtitre plate method developed in our group.[32] The pK_a values determined with the T3 apparatus were highly consistent (SD $<$ 0.03, n = 3) whereas the 96-well microtitre plate method gave somewhat less precise results (SD = 0.02–0.45, $n \geq 3$) (Table 1).

A good correlation (r^2 = 0.993) was observed between the pK_a values measured using spectrophotometry and potentiometry (Fig. 2A). The pK_a differences observed between both experimental techniques were generally $\leq$0.3 pK_a units except for compounds **1a** (+0.67), **4a** (+0.37), **5a** (+0.57), **20a** (+0.51), **21a** (+0.47), and **22b** (+0.41).

It is known that low aqueous solubility and chromophore strength can affect the accuracy of experimental pK_a determination for certain bases.[34] As all the compounds with greater discrepancies between UV-metric and pH-metric pK_a values have weak chromophores, this could explain the lack of accuracy with these compounds. In contrast, if we take the nitro derivatives **11a–15a** as an example of compounds with a strong chromophore and a smooth transition from the protonated ($\lambda_{max} \approx$ 298 nm at pH 3) to the neutral form ($\lambda_{max} \approx$ 364 nm at pH 12), we observe an excellent correlation between the UV-metric and pH-metric values (Table 1).

The pK_a values calculated using the AIBLHiCoS methodology correlated well (r^2 = 0.965) with the experimental results obtained using pH-metric titrations (see Fig. 2B) with deviations $<$0.30 pK_a units for the phenyl-imidazolidine derivatives. However, some deterioration was observed for pyridinyl compounds ($<$0.58) and two compounds containing nitro groups, **13a** (−0.79) and **15a** (−0.62), were also poorly predicted and are discussed in the next section. The mean absolute error (MAE) was found to be 0.23 with a standard deviation of 0.22 for the error values using the model which returned the highest validation statistics during calibration (C–N(im), Fig. S1, ESI†). This may be compared to the MAE value for ChemAxon predictions using the imino tautomer, which was found to be 0.77, with a standard deviation of 0.47 (Table S1 in the ESI†). The prediction power with the guanidine set of compounds was slightly lower with an MAE of 0.29, and most deviations $\leq$0.24 pK_a units except for compounds **17b** (−0.55), **24b** (+0.70) and one very high error for **22b** (+1.05), which will also be discussed in the next section (Table S2, ESI†).

Finally, with respect to the UV-metric pK_a values, deviations $\leq$0.52 pK_a units were observed against the predictions of AIBLHiCoS (and r^2 = 0.947) with the exception of compounds **5a** (+0.58), **13a** (−0.94), **15a** (−0.58), **21a** (+0.56) and **22a** (−0.59) (Fig. 2C).

2.3. Validation of the AIBLHiCoS prediction method applied to arylguanidines and 2-(arylimino)imidazolidines

The bond length *vs.* pK_a model used for most of the imidazolidine predictions in this work was chosen on the basis of its superior r^2, leave-one-seventh-out-q^2 and Root Mean Error of Estimation (RMSEE) values compared to a number of other candidate bond length models. For the 22 compounds of the training set (listed **1i–22i** in Table S3, ESI†), the highest validation statistics correspond to a model constructed using a C–N bond length of the imidazolidine ring, when compounds were represented as the imino tautomer ''T3''. This model is labelled C–N(im) in Fig. S1 (ESI†) and will be referred to as such throughout the following discussion. The second best validation statistics were observed for the N–C(Ph) bond, which is also labelled as such in Fig. S1 (ESI†). Predictions using both models are also listed in Table 1.

For guanidines, superior validation statistics for the training set (listed **g1–g13** in Table S4, ESI†) were obtained using the C=N bond length with compounds represented as amino tautomer ''A'', as illustrated in Fig. S2 (ESI†). All predictions listed in Table 1 and Table S2 (ESI†) were obtained using this model.

A high degree of prediction accuracy in modern terms is considered to be within 1 pK_a unit per prediction, with a mean absolute error (MAE) for a test set of less than 0.5 units.[35] As the

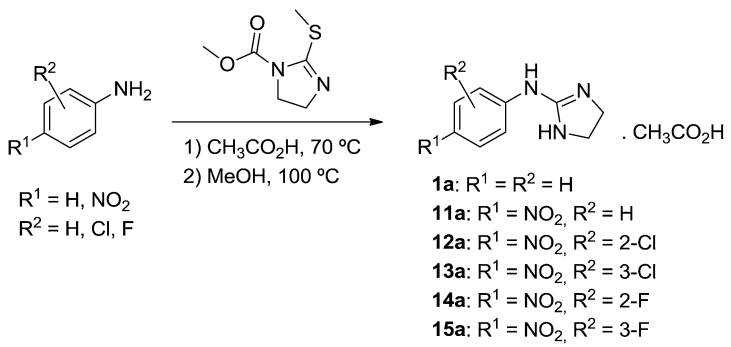

Scheme 2 Synthesis of **1a** and **11a–15a**.

Table 1 pK_a values of aryl/pyridinyl guanidines and iminoimidazolidines calculated using AIBLHiCos and determined experimentally by potentiometric and spectrophotometric methods

Cmpd	Structure	Predicted pK_a C–N(im)[a] pK_a N–C(Ph)[d]	pH-metric pK_a[b]	UV-metric pK_a[c]
1a	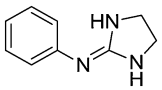	10.54 *9.90*	10.24 ± 0.001	10.91 ± 0.10
2a	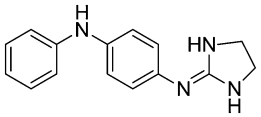	10.34 *9.89*	10.49 ± 0.01	—
3a	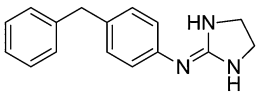	10.16 *9.78*	10.29 ± 0.01	10.40 ± 0.13
4a	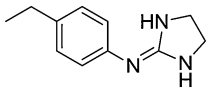	10.33 *9.89*	10.42 ± 0.001	10.79 ± 0.10
5a	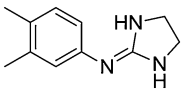	10.49 *9.94*	10.50 ± 0.01	11.07 ± 0.15
6a	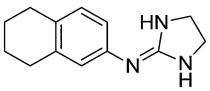	10.54 *9.97*	10.44 ± 0.01	10.27 ± 0.17
7a	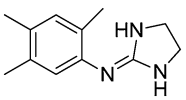	10.76 *10.26*	10.78 ± 0.01	10.91 ± 0.09
8a	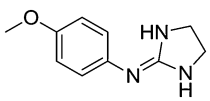	10.67 *10.16*	10.62 ± 0.01	10.80 ± 0.13
9a	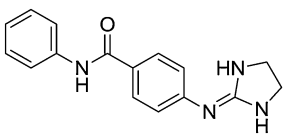	10.16 *9.73*	10.17 ± 0.01	10.28 ± 0.45
10a	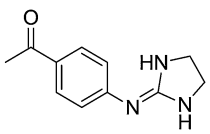	8.90 *8.79*	9.11 ± 0.001	9.42 ± 0.02
11a	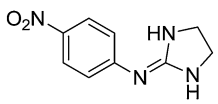	8.54 *8.26*	8.52 ± 0.001	8.37 ± 0.06
12a	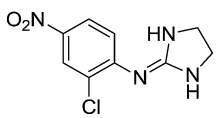	7.28 *7.48*	7.29 ± 0.07[e]	7.33 ± 0.03
13a	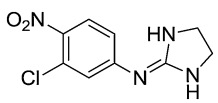	7.28 *8.01*	8.07 ± 0.001	8.06 ± 0.07
14a	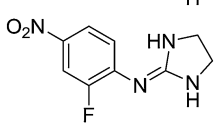	7.60 *7.32*	7.41 ± 0.001	7.41 ± 0.02
15a	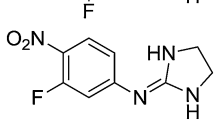	7.18 *7.89*	7.80 ± 0.001	7.69 ± 0.06

Table 1 (*continued*)

Cmpd	Structure	Predicted pK_a C–N(im)[a] pK_a N–C(Ph)[d]	pH-metric pK_a[b]	UV-metric pK_a[c]
16a	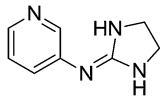	9.50 *9.30*	8.99 ± 0.001 3.05 ± 0.01[f]	8.99 ± 0.24 3.11 ± 0.17
17a	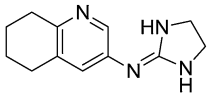	9.95 *9.54*	9.37 ± 0.001 4.36 ± 0.001[f]	9.57 ± 0.32 4.37 ± 0.19
18a	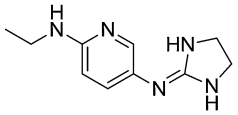	10.63 *10.02*	10.33 ± 0.001 4.97 ± 0.001[f]	10.35 ± 0.42 4.96 ± 0.08
19a	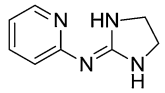	9.17 *7.65*	9.45 ± 0.001[g]	9.60 ± 0.06
20a	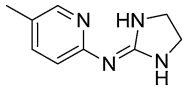	9.46 *7.81*	9.47 ± 0.01[g]	9.98 ± 0.05
21a	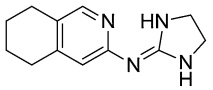	9.59 *7.91*	9.68 ± 0.001[g]	10.15 ± 0.15
22a	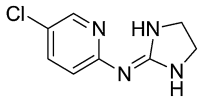	8.51 *7.30*	8.97 ± 0.001[g]	9.10 ± 0.09
23a	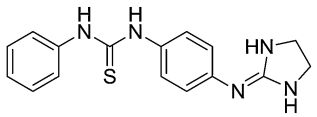	8.83 *9.14*	9.08 ± 0.01[e]	9.26 ± 0.06
1b	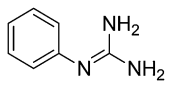	11.01	10.90 ± 0.001[h]	—
2b	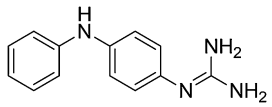	11.22	11.36 ± 0.01	—
3b	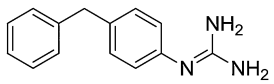	11.10	10.98 ± 0.001	10.95 ± 0.25
6b	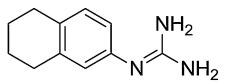	11.15	10.98 ± 0.001	—
7b	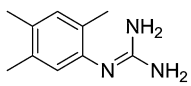	11.24	11.35 ± 0.01	—
17b	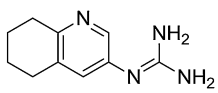	10.60	10.05 ± 0.001 4.44 ± 0.001[f]	N/A 4.13 ± 0.35
18b	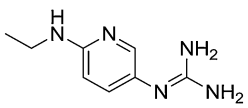	10.77	11.01 ± 0.01 4.94 ± 0.01[f]	N/A 4.98 ± 0.09
22b	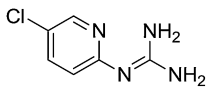	10.52	10.47 ± 0.001[g]	10.88 ± 0.08
24b	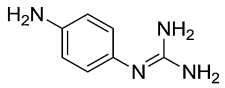	11.31	12.01 ± 0.03 3.63 ± 0.001	—

Table 1 (*continued*)

Cmpd	Structure	Predicted pK_a C–N(im)[a]	pK_a N–C(Ph)[d]	pH-metric pK_a[b]	UV-metric pK_a[c]
25b	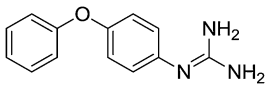	11.79		11.68 ± 0.01	11.70 ± 0.09
26b	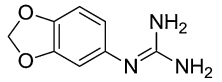	10.89		11.03 ± 0.01	11.23 ± 0.15
27b	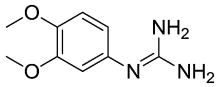	11.03		11.01 ± 0.01	11.12 ± 0.15

[a] Calculated using the AIBLHiCos approach with the C–N(im) bond model of the imino tautomer. [b] pH-metric determination at 25 °C using Sirius T3 apparatus. Mean of 3 titrations ± SD. [c] Determined by UV-spectrophotometry at 30 °C using the 96-well microtiter plate method.[32] Mean of ≥ 3 titrations ± SD. [d] Bond length model built from the same imidazolidine training set with compounds in the imino tautomeric form, but with the C–N(Ph) bond length connecting 2-iminoimidazolidine to benzene. [e] p$_s K_a$ measured with MeOH as a co-solvent (Yasuda–Shedlowsky extrapolation in H_2O). [f] pK_a value of the pyridin-3-yl nitrogen. [g] The pK_a value of the pyridin-2-yl nitrogen could not be worked out. [h] Literature: pK_a = 10.77.[33]

training sets consist of pK_a values taken from various sources, and therefore contain measurements obtained using different techniques, noise within the experimental datasets is to be expected. Small variations in conditions are also possible, *i.e.* solvent purity, sample purity and lab temperature, which can also have an effect on the values measured. According to the above conditions, the error statistics for both test sets show that both the guanidine and imidazolidine AIBLHiCoS models perform well. On only one occasion does any error exceed 1 unit, and the MAE values for both test sets are well below 0.5 (0.23 for imidazolidines and 0.29 for guanidines). For predictions made using the pK_a predictor plug-in within the Marvin Suite by ChemAxon,[36] with the imino tautomer as the input structure (Tables S1 and S2, ESI†), nine prediction errors exceed 1.0 pK_a units and the MAE values are in excess of 0.5 units for both imidazolidines and guanidines (0.77 and 0.54). AIBLHiCoS therefore finds its place here as a useful tool in instances where the empirical tools with a wider applicability radius struggle, as is the case for these guanidine-type ionisable groups.

2.3.1. Imidazolidines. A particular instance of where AIBLHiCoS performs notably well compared to ChemAxon is for the imidazolidine compounds **11a–15a**, all of which contain nitro groups at the *para* position of the phenyl ring. ChemAxon underestimates the acidity of these compounds by +1.23, +1.64, +1.18, +1.23 and +1.41 units, whereas the AIBLHiCoS model provides errors of +0.02, +0.01, −0.79, +0.19 and −0.62.

However, two of the largest prediction errors of the imidazolidine test set correspond to those for **13a** and **15a**, 2-(3-chloro-4-nitrophenylamino) and 2-(3-fluoro-4-nitro-phenylamino)imidazolidine. Errors for the pH-metric measurements are −0.79 and −0.62, and compared to the UV-metric values they also give errors of −0.94 and −0.58. The resonance-induced strong electron-withdrawing effect of nitro groups is known to perturb active bond lengths to such an extent that compounds containing these groups often form their own separate HiCoS.[28,29] Contrary to the previous results, the partitioning of the imidazolidine set into more structurally specific subsets may not be defined in this case by the presence of a nitro group at the *para*-position. This is explained by the fact that compound **7i**, (2-(2,6-Cl_2,4-NO_2-phenylimino)imidazolidine), is present within the training set used to form the predictive HiCoS, and **11a**, **12a** and **14a** of the test set fall in the expected region of the trend line for the LFER, as illustrated by their low prediction errors. According to the LFER exhibited between the C–N(im) bond length and pK_a, a shorter equilibrium bond length simply corresponds to a lower pK_a. In the case of **13a** and **15a**, we therefore observe an anomalously short C–N(im) bond, resulting in lower pK_a values than we would expect according to the LFER exhibited by most other congeners.

Looking to the optimised structures for **13a** and **15a** to explain these short bond lengths reveals the presence of an interaction between the O^- atom of the *p*-nitro group, and the *m*-Cl (**13a**) and *m*-F (**15a**) atoms. As a result of this interaction, the nitro group is seen to adopt a geometry whereby it is no longer co-planar with benzene. It may be asserted that the presence of this substituent interaction and deviation in nitro geometry, which is absent in all remaining *p*-nitro compounds, may be the cause of the anomalously short C–N(im) bond lengths.

The internal and external validation statistics for the chosen model (C–N(im)) are superior to any other bond length *vs.* pK_a plot (r^2 = 0.97, q^2 = 0.96 and RMSEE = 0.23). The next best model according to these validation statistics is observed for the same imidazolidine training set with compounds in the imino tautomeric form, but for the C–N bond length connecting benzene to 2-iminoimidazolidine (marked as N–C(Ph) within the structure labelled "T3" in Fig. S1, ESI†). This model has an r^2 value of 0.96, a q^2 value of 0.96 and a RMSEE value of 0.25. When the linear equation for this alternative model is used to predict for the whole test set **1a–23a**, the resultant MAE is significantly worse than the original model we chose to implement based on its superior statistics (the MAE is now 0.57 *vs.* 0.23).

For the 3-pyridyl compounds synthesized in this work, **16a–18a**, we observe errors of +0.51, +0.58 and +0.30 for the pH-metric measurements and −0.51, +0.38 and +0.28 for the UV-metric values. Despite the increase in MAE when the whole set is considered, use of the alternative N–C(Ph) model is seen to reduce the errors for **16a** and **17a** to −0.31 and +0.17. This improvement of predicted values can also be seen for the

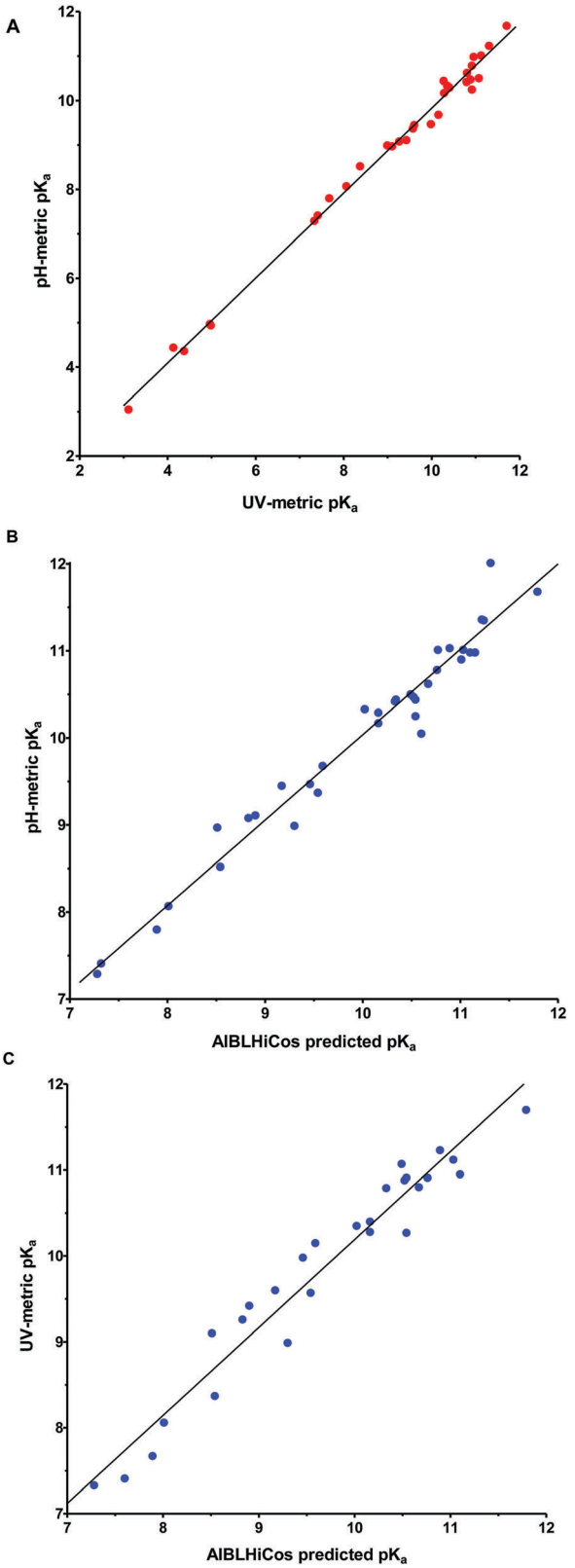

Fig. 2 (A) Correlation (r^2 = 0.993) between experimental pH-metric and UV-metric pK_a values for compounds **3a–23a**, **3b**, **17b**, **18b**, **22b**, **26b**, and **27b**. (B) Correlation (r^2 = 0.965) between pH-metric pK_as and AIBLHiCoS predicted pK_a values for compounds **1a–23a** and **1b–27b**. (C) Correlation (r^2 = 0.947) between UV-metric pK_as and AIBLHiCoS predicted pK_a values for compounds **3a–23a**, **3b**, **17b**, **18b**, **22b**, **26b**, and **27b**.

problematic nitro compounds, **13a** and **15a**, for which the errors decrease dramatically when predicted using the N–C(Ph) model (−0.26, +0.19, +0.06, −0.09 and +0.09 for **11a–15a**).

We now take a moment to briefly introduce the Interacting Quantum Atoms (IQA) energy partitioning scheme in accordance with the Quantum Theory of Atoms in Molecules (QTAIM).[37,38] By partitioning the total energy of a system into intra- and interatomic terms, it has been shown that we may derive a quantitative measure of covalent-like interactions between atoms in molecules. This comes in the form of the exchange–correlation potential energy V_{xc}^{AB}, which is the sum of the exchange energy V_x^{AB} and the correlation energy V_c^{AB}. The former term dominates V_{xc}^{AB}, and expresses the Fock–Dirac exchange, a consequence of the Pauli Principle, which describes the ever reducing probability of finding two electrons of the same spin as they approach each other (*i.e.* the Fermi hole). The latter term V_c^{AB} is associated with the Coulomb hole, which corresponds to the electrostatic repulsion between electrons. The absolute value of V_{xc}^{AB} between two atoms can be taken as the extent of delocalization of electrons between them, a factor that also determines the bond distance.

For the training set compounds, for C–N(im) and N–C(Ph), the V_{xc}^{CN} values (Table S5, ESI†) for the bonded atoms are found to have r^2 values of 0.990 and 0.992 with the corresponding bond lengths (Fig. S3(a) and (d), ESI†). However, the analogous plots for other bonds (marked "b" and "c" in Fig. S1 and (b and c) in Fig. S3, ESI†) have weaker correlations (r^2 = 0.939 and 0.897). Therefore, we can conclude that the bond lengths that correlate most highly with aqueous pK_a are those which are also most accurately reflecting the extent of delocalization between the two bonded atoms. Including the V_{xc}^{CN} *vs.* bond lengths for our outliers, **13a**, **15a**, **16a** and **17a**, shows that they do not diverge substantially from the highly correlated lines of the best fit for either C–N(im) or N–C(Ph). Correspondingly, these four compounds remain as outliers for the plot of V_{xc}^{CN} values *vs.* pK_a for C–N(im), and as observed for the bond lengths, fall within the expected region of the plot for V_{xc}^{CN} values *vs.* pK_a for N–C(Ph) (Fig. S4, ESI†).

On the basis of previous work, we suspect that for compounds with *m*-halogen and *p*-nitro substituents (**13a** and **15a**), the halo-nitro interaction perturbs the charge distribution of the guanidine fragment to such a degree that the relationship between C–N(im) and pK_a is no longer reflected in the general trend observed for most other congeners. If more pK_a data were available, it is proposed that we could form a new HiCoS consisting of only compounds of this type. Currently, in the absence of an adequate quantity of pK_a data, a separate predictive HiCoS using the C–N(im) bond lengths cannot be constructed. Given that the N–C(Ph) bond lengths and corresponding V_{xc}^{CN} values do not diverge from the general trend as a result of the halo-nitro interaction, the C–N(Ph) model should be used to predict compounds of this type. For two of three 3-pyridyl compounds (**16a–18a**), an explanation for their >0.5 prediction errors is not immediately accessible in terms of their structure. This is due to the fact that one 3-pyridyl containing compound, **18a**, has a relatively low error of +0.30 predicted

using the C–N(im) model. We can therefore assert that the presence of the heteroatom at the 3-position is not the sole cause of the higher pK_a values we predict, based on their longer C–N(im) bond lengths. Once again, in the absence of an adequate amount of experimental data for like compounds at the time of writing, we cannot prove indefinitely that these compounds would form their own subset. We therefore suggest that future predictions for all 3-pyridyl compounds be made *via* implementation of the N–C(Ph) model equation.

2.3.2. Guanidines. For the guanidine test set, the only AIBLHiCoS prediction above 1 unit corresponds to **22b**, 1-(5-chloro-2-pyridinyl)guanidine. Our model gives an error of +1.05 units whereas ChemAxon gives an error of −0.89. There are no pyridinyl-type compounds within the training set, but two 3-pyridinyls, **17b** and **18b**, return respectable errors of +0.55 and −0.24 using the C=N model. pK_a data for 1-(2-pyridinyl)guanidine and 1-(6-methyl-2-pyridinyl)guanidine are available, and when the bond lengths of their optimised structures are included in our C=N *vs.* pK_a plot using tautomer A (shown in Fig. S2 of the ESI,† bond labelled ii), they also appear below the line of the best fit, near the data point for **22b**. When predicted using the model equation, errors of +1.51 and +1.22 units are observed. It appears that the presence of the heteroatom at the 2-position of the aryl group causes further partitioning of the set once again. A new HiCoS cannot be constructed using only two data points, and so a predictive equation which would better describe the LFER for these compounds cannot be formulated until more pK_a data become available.

Boltzmann weighting of tautomers according to either internal or Gibbs energies at the level of theory used to obtain the bond lengths for the AIBLHiCoS protocol reveals a general prevalence of the "imino" tautomer for both sets of guanidines and imidazolidines. This tautomer is characterised by a C=N double bond between the central carbon atom of the Y-shaped guanidine

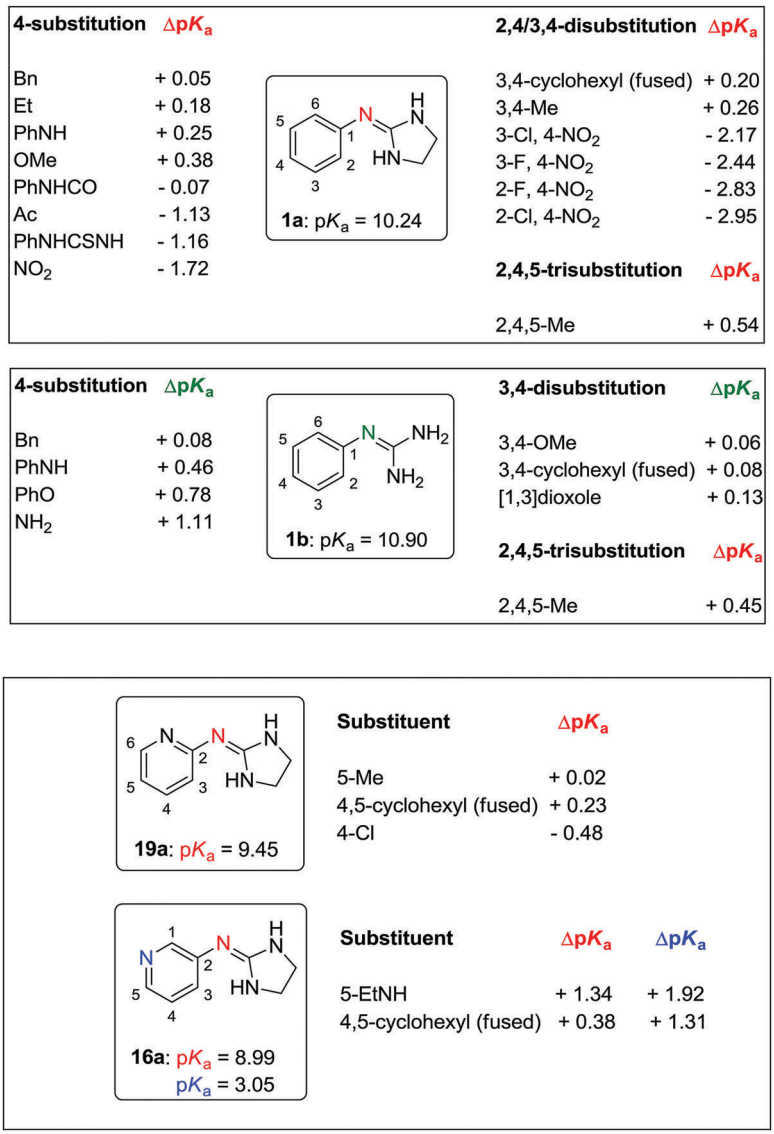

Fig. 3 Substituent effects on the pK_a of 2-(arylimino)imidazolidines and arylguanidines. The pK_a values were determined using potentiometric titrations at 25 °C. ΔpK_a is the difference in pK_a of the substituted compound with respect to the unsubstituted compound (**1a**, **1b**, **19a**, and **16a**, respectively).

fragment and the nitrogen adjacent to the phenyl group. For imidazolidines, the optimal model emerges from one of the C–N bond lengths of the 5-membered ring of this most stable tautomer. The emergence of the optimal model from the most stable tautomer is therefore congruent with it being the dominant species in solution, confirmed by the energetics. In terms of the ChemAxon predictions, using the most stable tautomer as an input structure allows for better prediction accuracy for both the imidazolidines and guanidines. However, for AIBLHiCoS the best internal validation statistics for guanidines are revealed using equilibrium bond lengths from a specific conformation of a higher energy tautomeric form, which is not in agreement with the energy rankings. Regardless of that these results corroborate those of our previous work,[27] which states that in the case of guanidines conformational commonality undermines stability; that is to say, as long as the compound of interest containing the guanidine group is optimised from this specific form, a very high degree of prediction accuracy may be obtained.

2.4. Quantitative effect of aryl substituents on the pK_a of aryl guanidines and 2-(arylimino)imidazolidines

According to a survey by Manallack on the pK_a distribution of drugs,[24] no CNS drug has a pK_a of above 10.5. Thus, phenylguanidine (**1b**: pK_a = 10.90), the reference compound in our study, is unlikely to have good CNS activity. Replacing the guanidine group of **1b** by a 2-iminoimidazolidine group (**1a**: pK_a = 10.24) leads to a drop in the basicity of the molecule ($\Delta pK_a = -0.66$). Changing the phenyl ring of **1a** for a 2-pyridinyl (**19a**) or a 3-pyridinyl (**16a**) group has a strong effect on the pK_a decrement ($\Delta pK_a = -0.79$ and -1.25, respectively). The effect of electron-donating and electron-withdrawing groups on the pK_a of 2-(arylimino)imidazolidines and arylguanidines is summarized in Fig. 3 and Table S6 (ESI†). As expected, these effects depend mainly on the capacity of these substituents to donate or withdraw electrons from the aryl ring, resulting in higher or lower electron density on the 2-imino nitrogen, respectively.

A linear relationship was found between the pK_a values and the Hammett σ values of *meta* and *para* substituents as shown in Fig. 4.[39,40] For *para*-amino substituents conjugated with the imidazolidine nitrogen (**2a**, **2b**, **24b**), σ_p^- values were used to get a good correlation. In contrast, compounds with an amide group (**9a**) in *para* position correlated poorly with the Hammett constant (red points in Fig. 4).

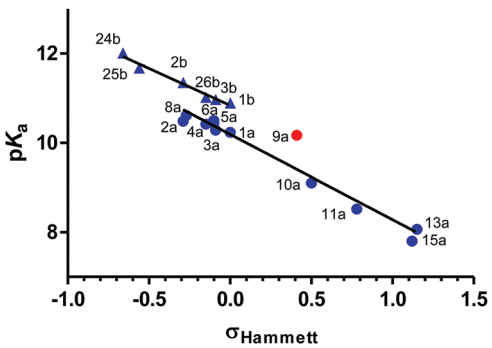

Fig. 4 Relationship between experimental pK_a (determined by potentiometric titrations at 25 °C) and Σ Hammett σ constants[39] for *meta* and *para* substituents of 2-(arylimino)imidazolidines (●) and arylguanidines (▲). Compounds that deviate significantly from the bottom (right) linear relationship appear in red (**9a**).

Amino substituents (**18a**, **18b**, **24b**) in the *para*-position to the guanidine/imidazoline group yield the strongest pK_a increase (ΔpK_a = +1.11 to 1.34), with the exception of the aminophenyl group (**2a**, **2b**), the electron donating capacity of which is much reduced by the presence of the phenyl ring (ΔpK_a = +0.25 to 0.46). Expectedly, the pK_a of the pyridine nitrogen is influenced to a larger extent by the presence of amino and alkyl electron-donating substituents (ΔpK_a = +1.31 and +1.92 for **17a** and **18a**, respectively). Alkoxy substituents (**8a**, **26b**, **27b**) have a smaller effect on the pK_a increase (ΔpK_a = +0.06 to 0.38) with respect to the phenoxy group (**25b**: ΔpK_a = +0.78). For electron-withdrawing substituents, the pK_a decrement follows this order: 4-PhNHCO < 4-Ac < 4-NO_2 < (3-Cl,4-NO_2) < (3-F,4-NO_2) < (2-F,4-NO_2) < (2Cl,4-NO_2). The addition of one halogen atom on the aryl ring results in pK_a decrements of 0.45 (3-Cl), 0.72 (3-F), 1.11 (2-F), and 1.23 (2-Cl). These values are consistent with the pK_a decrements measured for a series of chloro- and fluoro-substituted bis-2-(arylimino)-imidazolidines reported previously.[22]

Timmermans *et al.* have shown that the presence of two chlorine atoms in the position *ortho* to the 2-imino nitrogen reduces the pK_a value of the molecule by 1.66 units (*e.g.* 4-nitroclonidine: pK_a = 6.86 at 20 °C).[41] According to the pK_a values reported by Rozas and co-workers for a series of symmetric and unsymmetrical bisguanidines and bis-2-(phenylimino)imidazolidines,[42,43] the addition of a 4-imidazoline or 4-guanidine group on the phenyl substituent of **2a–b** and **3a–b** results in a pK_a decrement of approximately −0.50 units with respect to **2a–b** and **3a–b**. The values of ΔpK_a with respect to **1a–b** are shown in Fig. 5.

3. Conclusions

Arylguanidines and 2-(arylimino)imidazolidines whose pK_a values are reported here belong to a pharmacologically important class of molecules with promising applications as centrally active α_2-AR modulators. As the ionisation constant is a key physicochemical parameter that governs the membrane permeability of drugs (*e.g.* the BBB permeability in the case of CNS active compounds), the data of substituent effects on the basicity of arylguanidines and 2-(arylimino)imidazolidines can be useful for the design of new molecules of this class.

The dissociation constants of 23 arylguanidines and 12 2-(arylimino)imidazolidines measured using the spectrophotometry method were consistent with those measured using potentiometric titrations, further validating the 96-well microtitre plate method[32] as a useful tool for the medium throughput determination of pK_a of series of molecules.

Finally, we have shown that the AIBLHiCoS method is useful to predict the pK_a values of aryl guanidines and 2-(arylimino)-imidazolidines with low RMSD values, using only a single bond length obtained at a low level of theory. It must be noted that compound **12a** is an excellent example of the predictive power

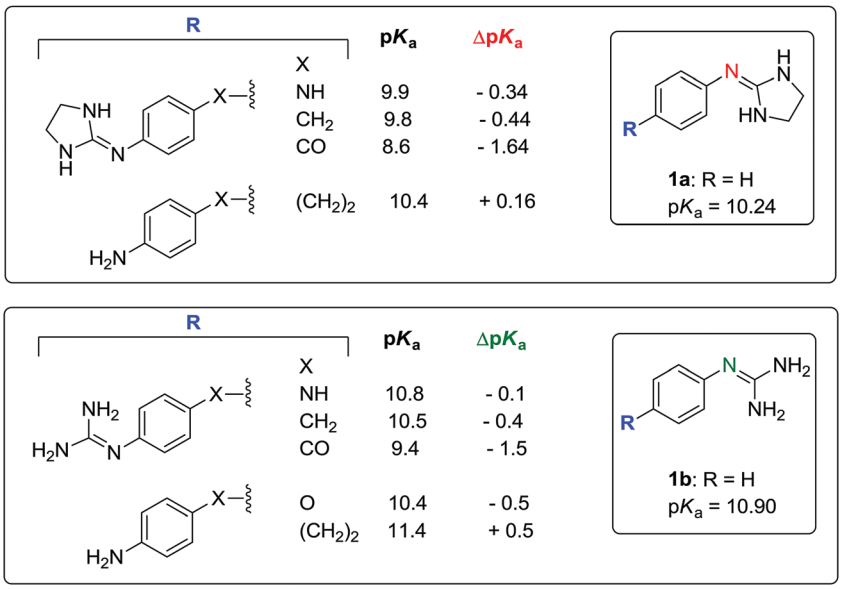

Fig. 5 Substituent effects on the pK_a of bis(2-(phenylimino)imidazolidines) and bisguanidines. Reported pK_a values determined using potentiometric[42] or UV-spectrophotometric[43] titrations at 25 °C. ΔpK_a is the difference in pK_a of the 4-substituted compound with respect to **1a** or **1b**.

of the AIBLHiCoS model. The initial (pH-metric) pK_a value we were working with was 8.13, meaning that our prediction of 7.28 was 0.85 units out, whilst for **14a**, the 2-fluoro analogue, the prediction error was only 0.19. Re-measurement of the pK_a value for **12a** then revealed the first to be erroneous, for reasons that are not clear, and the new pK_a value was observed to be 7.29, only 0.01 units out from the prediction. This value was also in excellent agreement with the UV-metric pK_a value (7.33).

4. Experimental

Chemistry

Melting points were measured in open capillary tubes using a Stuart Scientific SMP3 apparatus or a Mettler Toledo MP70 melting point system and are uncorrected. LC-MS spectra were recorded on a WATERS apparatus integrated with a HPLC separation module (2695), a PDA detector (2996) and a Micromass ZQ spectrometer. Analytical HPLC was performed with a SunFire C18–3.5 μm column (4.6 mm × 50 mm). Mobile phase A: CH_3CN + 0.08% formic acid and B: H_2O + 0.05% formic acid. UV detection was carried over 190 to 440 nm. Accurate mass was measured with an Agilent Technologies Q-TOF 6520 spectrometer using electrospray ionisation. ^{1}H NMR and ^{13}C NMR spectra were registered on Bruker Avance-300, Varian Inova-400, and Varian-system-500 spectrometers. Chemical shifts of the ^{1}H NMR spectra were referenced to the residual proton resonance of the deuterated solvents: D_2O (δ 4.79) and CD_3OD (δ 3.31). Chemical shifts of the ^{13}C NMR spectra were internally referenced for D_2O and CD_3OD (δ 49.0). Coupling constants J are given in hertz (Hz).

Synthesis of phenylguanidines (1b, 2b, 3b, 6b, 7b, and 24–27b) and 2-(phenylimino)imidazolidines (2a–10a, and 23a) as trifluoroacetate salts. The di-Boc-protected precursor[7] (typical scale: 5 to 25 mg) was dissolved in CH_2Cl_2 (1 mL) and CF_3CO_2H (0.5 mL) was added. The reaction was stirred for 4 h at room temperature and the volatiles were evaporated. Et_2O was added to the crude residue and evaporation was repeated. The TFA salts were obtained by precipitation from hexane/Et_2O (guanidines) or hexane (2-aminoimidazolines). The precipitates were rinsed with hexane and dried under high vacuum over P_2O_5 to yield the TFA salts as brownish hygroscopic solids. ^{1}H NMR spectra were consistent with the reported data.[7] Most of the compounds were ≥95% pure, or >90% (**4a**, **5a**, **6a**, **8a**, and **6b**, **7b**) as checked using HPLC-MS.

Synthesis of compounds 1a and 11a–15a. A Kimax tube charged with the aniline reagent (0.4 mmol, 1 equiv.) and methyl 2-(methylthio)-4,5-dihydro-1*H*-imidazole-1-carboxylate[31] (0.5 mmol, 1.25 equiv.) in glacial acetic acid (1.2 mL) was heated at 70 °C (1 day for **1a** and **13a**, 3 days for **11a** and **15a**) or 90 °C (4 days, **12a** and **14a**), until the formation of the methyl 2-(phenylamino)-4,5-dihydro-1*H*-imidazole-1-carboxylate intermediate. Then, methanol was added (1 mL) and the reaction was heated at 100 °C for 2 days (**1a**, **11a**, **13a**, **15a**) or 80 °C for 4 days (**12a**, **14a**). The solvent was evaporated under vacuum and the acetate salt of the product was isolated using silica chromatography (Isolute prepacked column, 2g). The non-polar starting materials were first eluted with 100% CH_2Cl_2, then the products were obtained with CH_2Cl_2 : MeOH (10 : 1) (compounds **1a**, **11a**, **13a**, **15a**) or CH_2Cl_2 : MeOH (15 : 1 → 10 : 1) (compounds **12a** and **14a**).

***N*-Phenyl-4,5-dihydro-1*H*-imidazol-2-amine acetate salt (1a).** Yellowish gum (88%). HPLC (UV) >92%. δ_H (300 MHz, D_2O) δ 7.44 (dq, J 2.9, 4.3, 6.0, 2H), 7.39–7.30 (m, 1H), 7.29–7.21 (m, 2H), 3.71 (s, 4H), 1.86 (s, 3H, AcO^-). δ_C (75 MHz, D_2O) δ 181.8 (AcO^-), 159.2, 135.4, 130.2, 127.8, 124.7, 43.0, 23.6 (AcO^-). MS (ESI^+) m/z 162 $(M + H)^+$.

***N*-(4-Nitrophenyl)-4,5-dihydro-1*H*-imidazol-2-amine acetate salt (11a).** Yellow-orangish solid (14%). Mp 190.2–193.1 °C.

HPLC (UV) >95%. δ_H (300 MHz, D_2O) δ 8.30 (d, *J* 9.1, 2H), 7.43 (d, *J* 9.1, 2H), 3.80 (s, 4H), 1.90 (s, 3H, AcO^-). δ_C (75 MHz, D_2O) δ 181.8 (AcO^-), 158.6, 145.1, 143.6, 125.9, 123.2, 43.1, 23.6 (AcO^-). MS (ESI^+) *m/z* 207 $(M + H)^+$. HRMS (ESI^+) *m/z* 206.0805 ($C_9H_{10}N_4O_2$ requires 206.0804).

***N*-(2-Chloro-4-nitrophenyl)-4,5-dihydro-1*H*-imidazol-2-amine acetate salt (12a).** Yellow solid (5%). Mp >195 °C. HPLC (UV) >95%. δ_H (400 MHz, D_2O) δ 8.54 (d, *J* 2.5, 1H), 8.30 (dd, *J* 2.5, 8.8, 1H), 7.73 (d, *J* 8.8, 1H), 3.85 (s, 4H), 1.95 (s, 3H, AcO^-). MS (ESI^+) *m/z* 241, 243 $(M + H)^+$. HRMS (ESI^+) *m/z* 240.0413 ($C_9H_9ClN_4O_2$ requires 240.0414).

***N*-(3-Chloro-4-nitrophenyl)-4,5-dihydro-1*H*-imidazol-2-amine acetate salt (13a).** Yellow solid (26%). Mp 156.5–160.3 °C. HPLC (UV) >95%. δ_H (300 MHz, D_2O) δ 8.10 (d, *J* 8.8, 1H), 7.55 (d, *J* 2.4, 1H), 7.35 (dd, *J* 2.4, 8.8, 1H), 3.81 (s, 4H), 1.89 (s, 3H, AcO^-). δ_C (75 MHz, D_2O) δ 181.7 (AcO^-), 158.3, 144.4, 141.6, 128.8, 128.2, 125.4, 121.6, 43.1, 23.6 (AcO^-). MS (ESI^+) *m/z* 241, 243 $(M + H)^+$. HRMS (ESI^+) *m/z* 240.0417 ($C_9H_9ClN_4O_2$ requires 240.0414).

***N*-(2-Fluoro-4-nitrophenyl)-4,5-dihydro-1*H*-imidazol-2-amine (14a).** Yellow solid (28%). Mp 220–226 °C. HPLC (UV) >95%. δ_H (500 MHz, methanol-d_4) δ 7.95 (dd, *J* 2.5, 8.7, 1H), 7.92 (dd, *J* 2.5, 10.7, 1H), 7.20 (t, *J* 8.7, 1H), 3.55 (s, 4H). δ_C (126 MHz, methanol-d_4) δ 161.9, 156.2 (d, *J* 246.6), 146.9 (d, *J* 11.5), 142.7 (d, *J* 8.7), 125.7 (d, *J* 3.3), 121.4 (d, *J* 3.0), 112.6 (d, *J* 25.9), 43.5. MS (ESI^+) *m/z* 225 $(M + H)^+$. HRMS (ESI^+) *m/z* 224.0706 ($C_9H_9FN_4O_2$ requires 224.0710).

***N*-(3-Fluoro-4-nitrophenyl)-4,5-dihydro-1*H*-imidazol-2-amine acetate salt (15a).** Yellow solid (24%). Mp 197.3–200 °C. HPLC (UV) >95%. δ_H (300 MHz, D_2O) δ 8.20 (t, *J* 8.7, 1H), 7.30 (dd, *J* 2.4, 12.5, 1H), 7.25–7.15 (m, 1H), 3.82 (s, 4H), 1.88 (d, *J* = 3.8, 3H). δ_C (75 MHz, D_2O) δ 181.7 (AcO^-), 158.4, 156.5 (d, *J* 242.5), 143.8 (d, *J* 13.1), 134.0 (d, *J* 9.4), 128.4, 118.0, 111.6 (d, *J* 24.6), 43.1, 23.5 (AcO^-). MS (ESI^+) *m/z* 225 $(M + H)^+$. HRMS (ESI^+) *m/z* 224.0707 ($C_9H_9FN_4O_2$ requires 224.0710).

Potentiometric pK_a determination. Titrations were carried out at 25 ± 0.5 °C in 0.15 M aqueous KCl solution under a nitrogen atmosphere using a SiriusT3 apparatus (Sirius Analytical Instruments Ltd, East Sussex, UK) equipped with an Ag/AgCl double junction reference pH electrode and a turbidity sensor. Standardised 0.5 M KOH and 0.5 M HCl were used as titration reagents. The KOH solution was standardized by potassium acid phthalate. The pK_a values are the mean of 3 titrations ±SD except otherwise noted.

Spectrophotometric p*K*a determination. The UV-spectra were recorded at 30 °C (*i.e.* room temperature) with a Thermo Multiskan spectrum apparatus using the 96-well microtiter plate method as described,[32] with the following modifications: (1) compounds' stock solutions were prepared in DMSO at *C* = 5 mM to ensure that the maximum absorbance of the compound was below 1.5 AU (*i.e.* the final concentration of the compound in the well was 0.1 mM). (2). The buffer solutions of constant ionic strength (0.1 M KCl) were prepared according to http://www.biomol.net/en/tools/buffercalculator.htm: (a) 25 mM phosphate buffer (pH 2.01, 2.54, 7.0, 7.27, 7.61, 7.94, 11.50, 11.80, and 12.40), (b) 25 mM citrate buffer (pH 3.23), (c) 25 mM acetate buffer (pH 4.17 and 4.61), (d) 25 mM MES buffer (pH 5.12, 5.66, 6.01, 6.19, 6.42, 6.62, and 6.78), (e) 25 mM ethanolamine buffer (pH 8.88, 9.17, 9.23, 9.66, 9.74, 10.13, and 10.32). The pH of the buffer solutions was measured at 30 °C (*i.e.* working temperature).

The raw UV data were processed using the Excel program (see the Excel sheet template in the ESI†) and the pK_a values were determined by linear regression from the total absorbance *vs.* pH curve as reported.[32] The pK_a values are the mean of 3 or 4 experiments (expressed as K_a values) ± SD.

Gas-phase *ab initio* calculations

The initial structures of each member of the respective training sets (guanidines and 2-(phenylamino)imidazolidines) were built using the program GaussView in each available tautomeric form. This equates to three tautomers for the imidazolidines, labelled T1–T3 in Fig. S1 (ESI†) and five ''tautomers'' for guanidines, labelled A–E in Fig. S2 (ESI†). For compounds with higher degrees of conformational freedom, several starting structures were generated using the ''Conformers'' plug-in within Marvin Sketch by ChemAxon.[35] Geometry optimization in the gas-phase was then performed for each conformer of each compound in each of the tautomeric forms using the GAUSSIAN09 program.[44] Calculations were initially carried out at the B3LYP/6-31G(d,p) level but the basis set was changed to 6-311G(d,p) for reasons that will be explained below. For biguanide derivatives included in the guanidine training set, various tautomeric forms of the guanidine fragment present within the *R* group were considered, whilst maintaining the specific tautomeric form of the guanidine fragment under consideration. Frequency calculations were carried out on optimised structures again using GAUSSIAN09, at the same level of theory. The output files were then inspected to confirm the absence of negative eigenvalues after diagonalization of the Hessian matrix, so that geometries are confirmed as true energy minima. Where a number of starting conformers of a tautomer were generated, the most stable conformer was chosen by comparing the total energies of each optimised structure. At this point we noticed that the chosen basis set was causing an issue in terms of ranking conformer stability between 2-(2-halogen-phenylimino)imidazolidine geometries with and without IHBs. These IHBs are seen to exist between an N–H group on imidazolidine and the *o*-halogen atom on benzene, and are ubiquitous throughout the most stable conformations of all compounds containing this substituent for tautomer T3, with the exception of 2-(2,4-Cl-phenylimino) and 2-(2,5-Cl-phenylimino)imidazolidine. This observation prompted the re-optimisation of all T3 training set compounds at the B3LYP/6-311G(d,p) level of theory. Using the valence triple zeta basis set revealed a consistent picture, where the presence of an IHB is a stabilising feature for all compounds. At this point all other calculations for T1 and T2 and tautomers A–E of the guanidine training set were also repeated for consistency. All analysis corresponds to the results of the calculations using the 6-311G(d,p) basis set.

Seven bond lengths were extracted from each imidazolidine compound, corresponding to each of the three CN bonds of the guanidine fragment, in addition to the N–C(Ph) bond connecting imidazolidine to benzene and the N–C, C–C and C–N bonds of

the imidazolidine ring. These are labelled a–g in Fig. S1 of the ESI.† Five bond lengths from within the guanidine moiety were also extracted, which correspond to the two CN single and one CN double bond of the guanidine group, the N–H bond attached to the imine nitrogen in A, B, D and E, and one N–H bond of a primary amine group. These are labelled i–v, in Fig. S2 (ESI†). The five bond lengths i–v within tautomers A–E were then regressed against the pK_a values for the set of guanidines. The seven bond lengths a–g of the three tautomers T1–T3 were also regressed against their pK_a values for the set of 2-(phenylimino)imidazolidines. The squared correlation coefficient (r^2), Root-Mean-Squared Error of Estimation (RMSEE) and leave-one-seventh-out q^2 values were obtained using the program SIMCA-P 10.0.[45]

By a comparison of internal and external validation metrics obtained for each bond length model, an optimal linear equation was chosen. For guanidines, the model was constructed using the C=N bond lengths of training set compounds as tautomer A, labelled ii in Fig. S2 (ESI†). For imidazolidines, the model was constructed using an endocyclic C–N bond length of the imino tautomer T3, labelled "a" in Fig. S1 (ESI†). The predictions for test set compounds **1a–23a** (2-(phenylimino)imidazolidines) and **1b–27b** (aryl guanidines) were obtained by energy minimization, (*via* a conformational search using Marvin followed by geometry optimisation), frequency calculations, and insertion of the appropriate bond length into the linear equation for the optimal bond length *vs.* pK_a model. The test compounds were constructed in the same tautomeric form as those of the training set used to construct the model.

The program AIMAll (version 14.04.17)[46] was used to carry out QTAIM analysis and the IQA partitioning calculations to obtain V_{xc} values for the atomic interactions corresponding to the C–N(im) and N–C(Ph) bonds. Calculations were carried out on B3LYP/6-311G(d,p) wavefunctions of the following species: the five nitro compounds (**11a–15a**), compound **11** of the training set and five compounds for which no pK_a data exists, 2-(3-Cl-phenylimino), 2-(3-F-phenylimino), 2-(3,5-Cl_2-4-NO_2-phenylimino), 2-(3-Br-4-NO_2-phenylimino) and 2-(3-F,5-Cl-4-NO_2-phenylimino)imidazolidine. For the five additional compounds, optimisation and frequency calculations were also performed at the B3LYP/6-311G(d,p) level before AIMAll analysis and the relevant bond lengths were extracted.

Conflicts of interest

There are no conflicts of interest to declare.

Acknowledgements

This work was supported by the Spanish Ministerio de Economia y Competitividad (Grant SAF2015-66690-R). B. A. Caine thanks BBSRC and Syngenta Ltd for PhD funding. P. L. A. P. acknowledges the EPSRC for funding through the award of an Established Career Fellowship (grant EP/K005472). We acknowledge the assistance of G. Romero and F. Peréz Gordillo (Instrumental Analysis Department at IQM) with the potentiometric pK_a measurements. We thank Chansèle Jourdan for her assistance with the UV-metric pK_a measurements. Dr Rozas is gratefully acknowledged for the gift of the pyridino derivatives **16–22** and the Boc-protected precursors of compounds **1–10** and **23–27**.

References

1 J. W. Shaw, D. H. Grayson and I. Rozas, *Topics in Heterocyclic Chemistry*, Springer Berlin Heidelberg, Berlin, Heidelberg, 2015, pp. 1–51, DOI: 10.1007/7081_2015_174.
2 P. O'Sullivan and I. Rozas, *ChemMedChem*, 2014, **9**, 2065–2073.
3 P. S. Nagle, C. McKeever, F. Rodriguez, B. Nguyen, W. D. Wilson and I. Rozas, *J. Med. Chem.*, 2014, **57**, 7663–7672.
4 P. S. Nagle, F. Rodriguez, B. Nguyen, W. D. Wilson and I. Rozas, *J. Med. Chem.*, 2012, **55**, 4397–4406.
5 P. S. Nagle, S. J. Quinn, J. M. Kelly, D. H. O'Donovan, A. R. Khan, F. Rodriguez, B. Nguyen, W. D. Wilson and I. Rozas, *Org. Biomol. Chem.*, 2010, **8**, 5558–5567.
6 P. S. Nagle, F. Rodriguez, A. Kahvedzic, S. J. Quinn and I. Rozas, *J. Med. Chem.*, 2009, **52**, 7113–7121.
7 F. Rodríguez, I. Rozas, M. Kaiser, R. Brun, B. Nguyen, W. D. Wilson, R. N. García and C. Dardonville, *J. Med. Chem.*, 2008, **51**, 909–923.
8 C. Dardonville, M. P. Barrett, R. Brun, M. Kaiser, F. Tanious and W. D. Wilson, *J. Med. Chem.*, 2006, **49**, 3748–3752.
9 C. Dardonville and R. Brun, *J. Med. Chem.*, 2004, **47**, 2296–2307.
10 C. Dardonville and J. J. Nué Martínez, *Curr. Med. Chem.*, 2017, DOI: 10.2174/0929867324666170623091522.
11 C. Millan, F. Acosta-Reyes, L. Lagartera, G. Ebiloma, L. Lemgruber, J. J. Nué Martinez, N. Saperas, C. Dardonville, H. de Koning and J. L. Campos, *Nucleic Acid Res.*, 2017, **45**, 8378–8391.
12 C. Dardonville, C. Fernandez-Fernandez, S. L. Gibbons, G. J. Ryan, N. Jagerovic, A. M. Gabilondo, J. J. Meana and L. F. Callado, *Bioorg. Med. Chem.*, 2006, **14**, 6570–6580.
13 C. Dardonville, N. Jagerovic, L. F. Callado and J. J. Meana, *Bioorg. Med. Chem. Lett.*, 2004, **14**, 491–493.
14 C. Dardonville, I. Rozas, P. Goya, R. Giron, C. Goicoechea and M. I. Martin, *Bioorg. Med. Chem.*, 2003, **11**, 1283–1291.
15 A. Alsasua, M. J. Borrego, M. T. Dannert, C. Dardonville, M. Rozas and M. I. Martin, *Fundam. Clin. Pharmacol.*, 2001, **15**, 84.
16 B. Kelly, M. McMullan, C. Muguruza, J. E. Ortega, J. J. Meana, L. F. Callado and I. Rozas, *J. Med. Chem.*, 2015, **58**, 963–977.
17 C. Muguruza, F. Rodriguez, I. Rozas, J. J. Meana, L. Uriguen and L. F. Callado, *Neuropharmacology*, 2013, **65**, 13–19.
18 F. Rodríguez, I. Rozas, J. E. Ortega, A. M. Erdozain, J. J. Meana and L. F. Callado, *J. Med. Chem.*, 2008, **51**, 3304–3312.
19 F. Rodriguez, I. Rozas, J. E. Ortega, J. J. Meana and L. F. Callado, *J. Med. Chem.*, 2007, **50**, 4516–4527.
20 F. Rodriguez, I. Rozas, J. E. Ortega, A. M. Erdozain, J. J. Meana and L. F. Callado, *J. Med. Chem.*, 2009, **52**, 601–609.
21 C. Dardonville and I. Rozas, *Med. Res. Rev.*, 2004, **24**, 639–661.

22 C. H. Rios Martinez, J. J. Nue Martinez, G. U. Ebiloma, H. P. de Koning, I. Alkorta and C. Dardonville, *Eur. J. Med. Chem.*, 2015, **101**, 806–817.
23 C. Ríos Martínez, F. Miller, K. Ganeshamoorthy, F. Glacial, M. Kaiser, H. de Koning, A. Eze, L. Lagartera, T. Herraiz and C. Dardonville, *Antimicrob. Agents Chemother.*, 2015, **59**, 890–904.
24 D. T. Manallack, *Perspect. Med. Chem.*, 2007, **1**, 25–38.
25 C. Anstöter, B. A. Caine and P. L. A. Popelier, *J. Chem. Inf. Model.*, 2016, **56**, 471–483.
26 I. Alkorta and P. L. A. Popelier, *ChemPhysChem*, 2015, **16**, 465–469.
27 M. Z. Griffiths, I. Alkorta and P. L. A. Popelier, *Mol. Inf.*, 2013, **32**, 363–376.
28 A. P. Harding and P. L. A. Popelier, *Phys. Chem. Chem. Phys.*, 2011, **13**, 11283–11293.
29 A. P. Harding and P. L. A. Popelier, *Phys. Chem. Chem. Phys.*, 2011, **13**, 11264–11282.
30 B. Kelly, M. McMullan, C. Muguruza, J. E. Ortega, J. J. Meana, L. F. Callado and I. Rozas, *J. Med. Chem.*, 2015, **58**, 963–977.
31 S. R. Mundla, L. J. Wilson, S. R. Klopfenstein, W. L. Seibel and N. N. Nikolaides, *Tetrahedron Lett.*, 2000, **41**, 6563–6566.
32 C. H. Ríos Martínez and C. Dardonville, *ACS Med. Chem. Lett.*, 2013, **4**, 142–145.
33 T. L. Davis and R. C. Elderfield, *J. Am. Chem. Soc.*, 1932, **54**, 1499–1503.
34 L. Settimo, K. Bellman and R. M. A. Knegtel, *Pharm. Res.*, 2014, **31**, 1082–1095.
35 A. D. Bochevarov, M. A. Watson, J. R. Greenwood and D. M. Philipp, *J. Chem. Theory Comput.*, 2016, **12**, 6001–6019.
36 MarvinSketch, version 6.2.2, calculation module developed by ChemAxon, http://www.chemaxon.com/products/marvin/marvinsketch/, 2014.
37 P. L. A. Popelier, *Atoms in Molecules. An Introduction*, Pearson Education, London, UK, 2000.
38 R. F. W. Bader, *Atoms in Molecules. A Quantum Theory*, Oxford Univ. Press, Oxford, UK, 1990.
39 C. Hansch, A. Leo and R. W. Taft, *Chem. Rev.*, 1991, **91**, 165–195.
40 L. P. Hammett, *J. Am. Chem. Soc.*, 1937, **59**, 96–103.
41 P. B. Timmermans and P. A. van Zwieten, *Arzneimittelforschung*, 1978, **28**, 1676–1681.
42 G. K. Kinsella, F. Rodriguez, G. W. Watson and I. Rozas, *Bioorg. Med. Chem.*, 2007, **15**, 2850–2855.
43 P. Nagle, A. Kahvedžić, T. McCabe and I. Rozas, *Struct. Chem.*, 2011, 1–9.
44 M. Frisch, G. Trucks, H. B. Schegel, G. Scuseria, M. Robb, J. Cheeseman, G. Scalmani, V. Barone, B. Mennucci and G. Petersson, *et al.*, *GAUSSIAN 09*, 2009.
45 UMETRICS, in SIMCA-P 10.0, www.umetrics.com, Umeå, Sweden, 2002.
46 T. A. Keith, *AIMAll*; TK Gristmill Software, Overland Park, KS, 2016, available at: http://aim.tkgristmill.com, accessed 1 May 2017.